

Provided for non-commercial research and education use.
Not for reproduction, distribution or commercial use.



This article appeared in a journal published by Elsevier. The attached copy is furnished to the author for internal non-commercial research and education use, including for instruction at the authors institution and sharing with colleagues.

Other uses, including reproduction and distribution, or selling or licensing copies, or posting to personal, institutional or third party websites are prohibited.

In most cases authors are permitted to post their version of the article (e.g. in Word or Tex form) to their personal website or institutional repository. Authors requiring further information regarding Elsevier's archiving and manuscript policies are encouraged to visit:

<http://www.elsevier.com/authorsrights>



Contents lists available at SciVerse ScienceDirect

Remote Sensing of Environment

journal homepage: www.elsevier.com/locate/rse

Assimilation of multiple data types for improved heat flux prediction: A one-dimensional field study

R.C. Pipunic^{a,*}, J.P. Walker^b, A.W. Western^a, C.M. Trudinger^c^a Department of Infrastructure Engineering, The University of Melbourne, Parkville, Vic 3010, Australia^b Department of Civil Engineering, Monash University, Clayton, Vic 3800, Australia^c CSIRO Marine and Atmospheric Research, Centre for Australian Weather and Climate Research, PMB 1 Aspendale, Vic 3195, Australia

ARTICLE INFO

Article history:

Received 18 February 2011

Received in revised form 21 May 2013

Accepted 22 May 2013

Available online xxx

Keywords:

Data assimilation

Ensemble Kalman filter

Land surface model

Latent and sensible heat flux

Skin temperature

Soil moisture

ABSTRACT

Accurate latent (LE) and sensible (H) heat flux partitioning from Land Surface Models (LSMs) is important for numerical weather prediction. Land data assimilation can play a key role in improving heat flux prediction by merging information from a range of remotely sensed products with LSMs. This paper demonstrates this potential for an open grassland site in Australia via one-dimensional experiments spanning a year-long period. With a focus on how a LSM is impacted, in-situ field observations were assimilated. Data types as available from passive microwave and thermal infra-red remote sensors were tested for their impact, with individual and joint assimilation of LE and H , near-surface soil moisture, and skin temperature observations—all on time scales approximating satellite overpass intervals. Assessed against independent data from field observations, the multi-observation approach of joint near-surface soil moisture and skin temperature assimilation made the greatest improvements to LE (expressed as daily evapotranspiration; ET), being slightly better than for joint LE and H assimilation. This result questions the value of using LE and H retrievals from thermal imagery within an assimilation context. Individually, skin temperature assimilation was one of the best performers for soil temperature estimates but with degraded root-zone soil moisture estimates and minimal ET improvements. Likewise, near-surface soil moisture assimilation produced the greatest root-zone soil moisture improvement but with relatively modest ET improvement. Combined near-surface soil moisture and skin temperature assimilation balanced the improvements to both soil moisture and temperature states along with strong improvements to ET estimates, highlighting the benefits of multi-observation assimilation.

Crown Copyright © 2013 Published by Elsevier Inc. All rights reserved.

1. Introduction

Land Surface Models (LSMs) require careful initialisation in order to achieve accurate latent (LE) and sensible (H) heat flux prediction. Relative humidity and temperature in the lower atmosphere are influenced by LE and H from the land surface (Denman et al., 2007), and hence LSM state initialisation impacts Numerical Weather Prediction (NWP) model skill (Beljaars et al., 1996; Case et al., 2008; Chen et al., 2001, 2007; Koster et al., 2004). Due to spatial and temporal land surface heterogeneity and the resulting complexity of water and energy exchanges between soil, vegetation, and the atmosphere, characterising these interactions with LSMs is inherently uncertain. Thus a challenge for NWP is to obtain the most accurate LE and H predictions from LSMs whilst maintaining realistic model physics and state estimates. Global coverage and regular temporal repeat of land surface state and flux quantities from current and emerging remote sensing data provides an opportunity to meet this challenge through data assimilation, the process whereby such information is

combined with model estimates (factoring in uncertainty estimates for each) to produce the best predictions possible.

Remotely sensed information relevant to LSMs includes microwave brightness temperature, which is related to soil moisture content (e.g. Gao et al., 2006; Njoku & Entekhabi, 1995) and forms the basis of global soil moisture data products such as those derived from Advanced Microwave Scanning Radiometer (AMSR-E/AMSR2) data (Imaoka et al., 2010; Owe et al., 2008) or the European Space Agency's Soil Moisture and Ocean Salinity (SMOS) data (Kerr, 2001). Active microwave sensor data such as from the Advanced Scatterometer (ASCAT) are also valuable for deriving soil moisture content (Wagner et al., 1999) and have been used for assimilation research in an NWP context (e.g. Mahfouf, 2010), including use for testing a newly implemented assimilation scheme in an operational system (de Rosnay et al., 2012) and for operational forecasting (Dharssi et al., 2011). Thermal infra-red (TIR) data provide information on skin temperature and hence model soil temperature states, which are an important part of the land surface energy and water balance (Entekhabi et al., 1994; Viterbo & Beljaars, 1995). Moreover, skin temperature based on data from sensors such as the Moderate Resolution Imaging Spectroradiometer (MODIS; e.g. Wan & Li, 1997) and Landsat Thematic Mapper (TM; e.g. Sobrino et al.,

* Corresponding author. Tel.: +61 3 8344 4893.

E-mail address: robp@unimelb.edu.au (R.C. Pipunic).

2004) can be combined with other remote sensing data to derive spatially distributed *LE* and *H* data products using algorithms such as METRIC (Allen et al., 2007), SEBS (Su, 2002), and SEBAL (Bastiaanssen et al., 1998).

In many coupled NWP systems soil moisture is treated as a tuning variable and adjusted in non-physical ways to produce fluxes that are congruent with atmospheric observations (Douville et al., 2000; Mahfouf, 1991; Rhodin et al., 1999; Seuffert et al., 2004). With the aim of achieving more physically realistic LSM predictions of soil states (i.e. soil moisture and temperature) and heat fluxes (i.e. *LE* and *H*), a common assumption is that more accurate root-zone soil moisture should lead to improved heat fluxes, due to the role of profile soil moisture in regulating the partitioning of available energy at the land surface (Reichle et al., 2007). To this end, and spurred by the emergence of remotely sensed soil moisture products, there has been considerable LSM assimilation research focusing on soil moisture.

The potential for improving root-zone soil moisture predictions with near-surface soil moisture assimilation (remote sensing products characterise the top few centimetres of soil at most) has been demonstrated via synthetic studies (Entekhabi et al., 1994; Kumar et al., 2009; Pipunic et al., 2008; Reichle et al., 2008; Walker & Houser, 2004). Real data on near-surface moisture has been assimilated in one-dimensional in-situ field experiments (Li & Islam, 1999; Sabater et al., 2008; Walker et al., 2001a). Experiments using remotely sensed products have also shown some potential in terms of improving root-zone soil moisture (Draper et al., 2009a; Reichle & Koster, 2005; Reichle et al., 2007), but few have demonstrated impacts on atmospheric prediction (Mahfouf, 2010). Skin temperature assimilation has also been investigated via synthetic experiments (e.g. Entekhabi et al., 1994; Pipunic et al., 2008) and real data experiments involving both in-situ field and remotely sensed data (Huang et al., 2008; Lakshmi, 2000; McNider et al., 1994; Meng et al., 2009; Reichle et al., 2010), showing promise for the improvement of model states and/or heat fluxes.

Assimilating combinations of different observation types is expected to provide better overall model constraint through direct impact on different variables simultaneously. Research into such strategies is important as the availability of different remotely sensed data increases. Examples include synthetic experiments for combined assimilation of observations relating to remotely sensed soil moisture and skin temperature by Entekhabi et al. (1994) and Balsamo et al. (2007) for an NWP context (whose study also incorporated screen-level variables). While Balsamo et al. (2007) assessed the contribution to atmospheric screen-level prediction from different observations, and highlighted the importance of soil state and land surface heat fluxes to screen-level prediction, neither study explicitly assessed land surface flux predictions.

Pan et al. (2008) assimilated both remotely sensed microwave brightness temperature (linked to soil moisture) and an *LE/ET* product. Assessed against independent model predictions there was improvement to soil moisture but not to *ET*, leading them to conclude that improvement from assimilating remotely sensed *ET* remains challenging. The strategy of assimilating heat flux observations has received minimal attention in literature. Other examples are limited to Schuurmans et al. (2003) who assimilated remotely sensed *ET* retrievals from the SEBAL algorithm (Bastiaanssen et al., 1998), showing impacts on modelled *ET* that appeared promising but with no independent data for validation, and the assimilation of both *LE* and *H* in a synthetic study by Pipunic et al. (2008) which showed improved flux predictions. Hain et al. (2012) assimilated soil moisture estimates which they retrieved using an *ET* product derived from TIR remote sensing, along with microwave based soil moisture estimates. However they did not explicitly assimilate *ET* itself and only evaluated assimilation impacts on modelled soil moisture, with the soil moisture data derived from the *ET* product making the best improvements to modelled root-zone moisture.

Current challenges with remotely sensed data assimilation include disparate spatial and temporal resolution between data sources available

for model input, assimilation and validation, and considerable errors in both remotely sensed products and models (Reichle et al., 2007). From an operational NWP perspective, the ultimate aim is to utilise available land surface and screen-level meteorological observations for assimilating into a system where the LSM and atmospheric model are coupled. The scope of this study covers only LSM assimilation, as it is important to thoroughly test a LSM offline first and understand the impacts (and limitations) from assimilating different data types—starting with point-scale scenarios where observational uncertainties from in-situ measurements are better understood, prior to testing in more complex spatial scenarios and coupled systems involving greater uncertainty.

This paper examines the impact from assimilating different data types on soil states and heat fluxes for the CSIRO Biosphere Model (CBM, Wang et al., 2001, 2007)—a version of the Community Atmosphere Biosphere Land Exchange (CABLE) model (Kowalczyk et al., 2006; Wang et al., 2011). The work presented here is an extension to the synthetic twin experiments of Pipunic et al. (2008) which demonstrated the potential of assimilating remotely sensed product types other than soil moisture to improve heat flux predictions. That study was based on simulations limited to a 3 month period forced with data from summer/early-autumn and with relatively uniform/sparse vegetation cover (LAI ~0.30–0.40). While it demonstrated that *LE*, *H* and skin temperature assimilation could provide comparable and/or better improvement to heat fluxes than near-surface soil moisture assimilation alone, it also showed that improved soil moisture predictions from near-surface soil moisture assimilation did not translate to the best overall *LE* and *H* predictions.

Here we extend on the proof-of-concept study of Pipunic et al. (2008) via year-long experiments spanning the full vegetation growth cycle and using real in-situ observations of *LE*, *H*, near-surface soil moisture and skin temperature. This includes combinations of observations that represent multi-sensor data assimilation approaches not examined in the synthetic study. While different temporal scales are taken into account, including the masking of optical data by cloud, this paper does not address the important issue of the contrasting spatial scales between optical and passive microwave products.

2. Modelling and assimilation

The CSIRO Biosphere Model (CBM, Wang et al., 2001, 2007) used in this study was developed in Australia by scientists at the Commonwealth Scientific and Industry Research Organisation (CSIRO), Marine and Atmospheric Research division. It was used for the synthetic study by Pipunic et al. (2008), and for consistency, was used in the extension of that work presented here. As a precursor to the current Community Atmosphere Biosphere Land Exchange (CABLE) model (Kowalczyk et al., 2006; Wang et al., 2011), which is planned for use as the LSM for Australia's NWP (Law et al., 2012), the CBM shares similar formulations for the land surface water and energy balances. The data assimilation scheme used for all experiments in this study was the Ensemble Kalman Filter (EnKF, Evensen, 1994).

A description of the CABLE model by Kowalczyk et al. (2006) provides details on the energy balance and soil scheme, which are very similar in the two versions (CBM and CABLE). The CBM soil profile has a total depth of 4.60 m and consists of six layers of fixed thickness which are (from the uppermost to the bottom layer): 2.2, 5.8, 15.4, 40.9, 108.5 and 287.2 cm. Soil moisture movement is only in the vertical direction between layers and is calculated based on Richard's equation, with individual prognostic soil moisture and soil temperature state variables being associated with each layer. However, only a single set of soil parameter values can be specified for all soil layers, resulting in uniform properties over the whole soil profile. Linking with the vegetation scheme is through the plant root distribution, where the percentage of roots in each soil layer can be specified by the user. Vegetation in the CBM is represented by a detailed two leaf canopy model—a “big” sunlit and a “big” shaded leaf

(Wang & Leuning, 1998)—which includes aerodynamic and radiative interaction between the ground and the vegetation (Raupach et al., 1997). Also included in the CBM are calculations for photosynthesis, leaf temperature, and stomatal conductance.

The Leaf Area Index (*LAI*) parameter plays a key role in determining the relative fraction of canopy cover to bare soil. Net radiation is calculated separately for the vegetation canopy and soil surface, as is *LE* and *H* where total *LE* and *H* outputs are the sum of the canopy and soil components. Total skin temperature from the CBM is based on a combination of the soil and canopy surface temperature components involved in longwave radiation balance calculations and is summarised as follows:

$$\sqrt[4]{\{[1.0 - f(LAI)] \times T_{can}^4\} + [f(LAI) \times T_{soil}^4]}. \quad (1)$$

The soil component (*Tsoil*) is the temperature state variable of the top-most soil layer (0–2.2 cm), while the canopy surface component (*Tcan*) is based on a non-prognostic leaf temperature variable which is determined iteratively at every model time step (after initialisation with air temperature from meteorological forcing) as part of the vegetation canopy energy balance calculations. Relative contributions from soil and vegetation components to the total skin temperature are determined by a weighting factor $f(LAI)$, which is a function of *LAI* that describes the fraction of radiation (from 0 to 1) transmitted through the canopy.

The aim with sequential data assimilation techniques, such as the EnKF used in this work, is to update and correct prognostic state variables, with an expectation that key diagnostic variables, such as heat fluxes, will consequently be improved. Updates were applied here to soil moisture and soil temperature states for each of the six CBM soil layers. In relation to heat fluxes, the top-most soil layer moisture and temperature states are closely related to the soil component of *LE*, while the soil moisture states for layers which have roots are used in a water availability term linked to the vegetation component of *LE*, and hence also indirectly linked to leaf temperature. The temperature state variable of the top-most soil layer is closely linked to calculations for the soil component of *H*, whereas the vegetation canopy component results from vegetation energy balance calculations, involving the vegetation component of *LE* and the non-prognostic leaf temperature variable (both indirectly linked to soil moisture). Details of the EnKF and its application to the CBM are contained in Pipunic et al. (2008).

For meaningful comparisons to be made between observation-based and LSM predicted state data as part of data assimilation, systematic biases must be removed (Drusch et al., 2005; Reichle & Koster, 2004). Bias can be due to representative differences, such as differences in soil depth or spatial scale between observations and model estimates, and also uncertainties specific to different sources of information. These include uncertain LSM parameters such as wilting point and field capacity (amongst others) which influence moisture dynamics (Koster & Milly, 1997), while observation-based data may have different dynamics as a result of a particular observing instrument or algorithm used to estimate final quantities from remotely sensed observations. Although instrument bias is typically of limited concern for well calibrated in-situ installations, the correct treatment of bias remains a challenge, particularly using LSMs and remotely sensed products in the absence of adequate information enabling its source(s) to be accurately identified and quantified.

Rescaling approaches such as cumulative distribution function (*cdf*) matching of observed data series to LSM state climatology prior to assimilation are now considered de rigueur for bias removal (e.g. Draper et al., 2009a; Drusch et al., 2005; Reichle & Koster, 2004). Reichle and Koster (2004) demonstrated that rescaling remote sensing derived surface soil moisture to model predictions for a one year period reduced observation-model bias over a subsequent nine year series, but did not fully remove it. This highlights the difficulty in thoroughly understanding and dealing with such bias, especially if only short data series are available. Keeping in line with current standard practice,

observation-model bias for land surface states in this study were eliminated by rescaling the observed data series prior to assimilation, by matching the mean and standard deviation to that of the CBM predicted series. In the long-term however, research effort should focus on better understanding and treating bias in LSMs which may involve improvements to model physics and/or better parameterisation—likewise for remotely sensed land data products given the ultimate aim is operational assimilation.

3. Study site and data

The one-dimensional modelling experiments presented in this paper were carried out for a flux station site in south eastern Australia, located on non-irrigated pasture within a mainly agricultural area at Kyeamba Creek (Fig. 1). Site instrumentation consisted of an eddy covariance system, meteorological sensors, soil moisture and soil temperature sensors. Smith et al. (2012) summarises the main instruments used and briefly describes the landscape of the Kyeamba Creek catchment. Key environmental characteristics and CBM parameter values that were used for modelling experiments here are summarised in Table 1.

This site was managed by this paper's lead author and no details have previously been published on the basic processing for this data, thus some are included herein. Kyeamba Creek is a tributary of the Murrumbidgee River, located in the south of Australia's Murray Darling Basin. The flux station location was on the alluvial flats of the creek valley approximately 20 km south east of an Australian Bureau of Meteorology (BoM) automatic weather station in the town of Wagga Wagga (Fig. 1). Heat fluxes, meteorological variables, soil moisture and soil temperature data were all measured for a full year period from January 1st to December 31st 2005 and processed to a 30 minute time-step. The total percentage of instrument down-time at the site was approximately 10%, with the longest consecutive gap being about 16 days from day of year (DoY) 59 to 75. Meteorological data gaps were in-filled using 30 minute meteorological data compiled from BoM Wagga Wagga automatic weather station data (Siriwardena et al., 2003), with the exception of rainfall for which supplementary data was available from an adjacent OzNet monitoring station (Smith et al., 2012) approximately 200 m away (<http://www.oznet.org.au/k10.html>). Corresponding gaps in the *LE*, *H*, soil moisture and soil temperature data series were not in-filled.

The *LE* and *H* were measured with an eddy covariance system consisting of a CSAT 3D sonic anemometer (Campbell Scientific Inc., 1998) and LI-7500 open path gas analyser (LI-COR Inc., 2003). They were elevated 3 m above the ground giving an approximate maximum fetch of 300 m. A CNR1 four-way net radiometer (Kipp & Zonen, 2002) measured the incoming and outgoing components of short and longwave radiation for determining the total net radiation at the land surface (R_N). Ground heat flux (*G*) was also measured using two HFT3 ground heat flux plates (Campbell Scientific Inc., 1999) buried 8 cm below the surface, and corrected to represent *G* at the land surface using temperature thermocouple and soil moisture measurements in the 0–8 cm layer of soil as outlined in the HFT3 manual (Campbell Scientific Inc., 1999).

The *LE* and *H* data were filtered for spurious values and conditions known to compromise the quality of 3D eddy covariance measurements (e.g. rainfall), and night time data (from 6 pm to 6 am) were discarded. The energy balance gap between ($LE + H$) and ($R_N - G$) was approximately 20% and the technique of Twine et al. (2000) was applied to achieve closure. This method adjusts *LE* and *H* to achieve a closed energy balance against measured ($R_N - G$) while maintaining a constant Bowen Ratio (H/LE). The root mean square error (RMSE) between the *LE* and *H* data before and after closing the energy balance was just under 40 Wm^{-2} for each.

Soil moisture observations were made over depths of 0–8 cm, 0–30 cm, 30–60 cm and 60–90 cm using CS615 water content reflectometer probes (Campbell Scientific Inc., 1996), and calibrated using a number of independent gravimetric and TRASE Time Domain

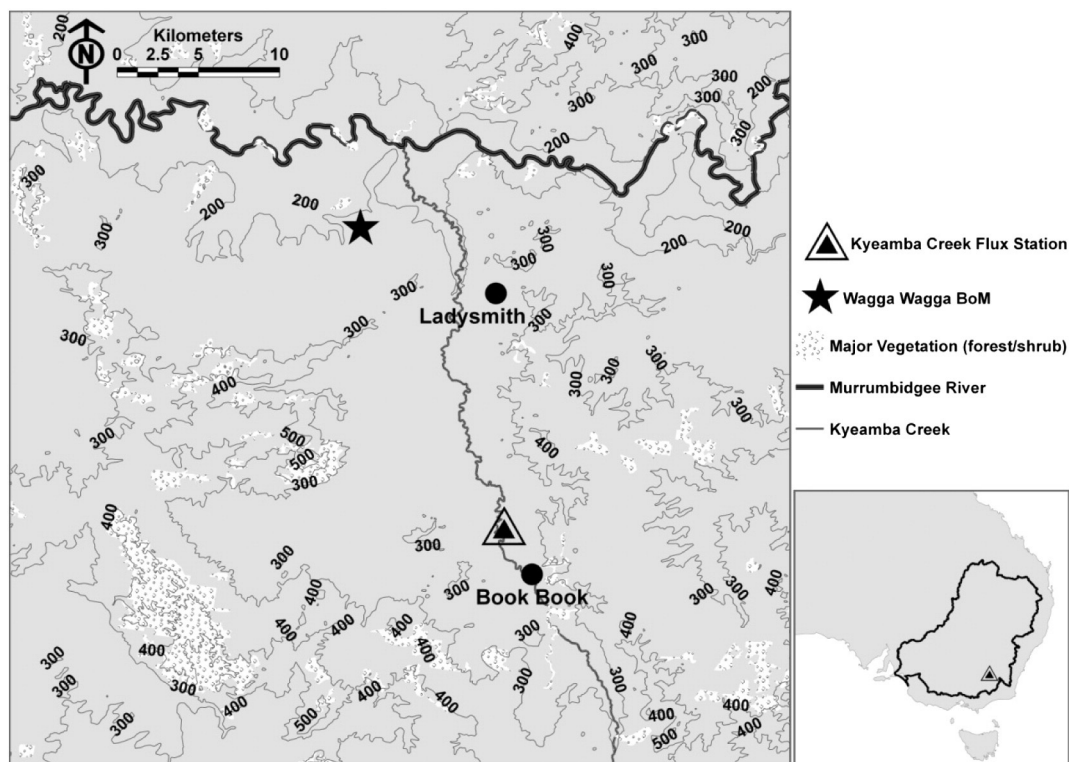


Fig. 1. Map showing locations of the Kyeamba Creek flux station study site, Wagga Wagga BoM automatic weather station, and NSW Office of Water discharge gauges for Kyeamba Creek near Ladysmith and Book Book. Grey elevation contour lines are in metres. The Oznet soil moisture and rainfall monitoring site is situated ~200 m west of the flux station. A broad scale overview of the Kyeamba Creek site location in south eastern Australia is shown in the bottom right hand corner with the black boundary delineating the Murray Darling Basin.

Reflectometer (TDR, Soil Moisture Equipment Corp., 1989) volumetric soil moisture measurements made under wet and dry conditions. After soil temperature correction of raw CS615 data following Western and Seyfried (2005), a calibration relationship was established with an accuracy of ~0.02 vol/vol. Soil temperature was measured at depths of 2 cm,

5 cm, 10 cm, 20 cm, 50 cm and 100 cm with Unidata 6507A temperature thermistor probes (Unidata Australia, 1997).

Table 1
Summary of Kyeamba Creek flux station site characteristics and key model input data relevant to numerical experiments.

Managing institution	The University of Melbourne
Location (WGS84)	147.56°E, -35.39°S
Elevation—metres above sea level	~233
Vegetation	Grass pasture (non-irrigated)
LAI range ^a	~0.25 (Summer/Autumn)–3.0 (Spring)
Average canopy height (m)	~0.25
Dominant soil type	Silty loam
Soil bulk density (kg/m ³)	1475
Soil porosity (vol/vol)	0.450
Soil field capacity (vol/vol)	0.360
Soil wilting point (vol/vol)	0.070
Soil hydraulic conductivity at saturation (m/s)	8.33×10^{-6}
Soil suction at saturation (m)	0.505
Long term average annual rainfall (mm/yr) ^b	~575
Spinup period (simulation repeated 12 times) ^c	Jan 1st 2004–Dec 31st, 2004;
Total rainfall (mm):	585
Experimental period ^d	Jan 1st 2005–Dec 31st, 2005;
Total rainfall (mm):	595

^a Based on AVHRR-derived monthly data used for simulations over 2004 and 2005.
^b For the period 1941–2012 at the Australian Bureau of Meteorology (BoM) Wagga Wagga station (http://www.bom.gov.au/climate/averages/tables/cw_072150.shtml) shown in Fig. 1.
^c Most of the meteorological forcing generated from BoM Wagga Wagga station data (Siriwardena et al., 2003), with rainfall data from the K10 Oznet station (Smith et al., 2012) ~200 m from the flux station site.
^d All data are site measured, with small gaps in the forcing in-filled using Wagga Wagga BoM data and rainfall gaps in-filled using the nearby K10 Oznet data (Smith et al., 2012).

The meteorological variables measured at the station include incoming short and longwave radiation, rainfall, air temperature, wind speed, saturation vapour pressure and station level barometric air pressure—specific humidity was derived from barometric air pressure and saturation vapour pressure. These were all used for model forcing over the experimental period (2005). Incoming short and longwave radiation used for forcing were measured with the two CNR1 upward facing sensors, whereas all four separate CNR 1 sensor measurements (upward and downward facing for both short and longwave) were combined for R_N to correct the LE and H data used for assimilation as described above. Thus the corrections to LE and H partly involved the same incoming radiation data used for CBM forcing, but also the separately measured outgoing short and longwave radiation and G which were not used for any model input or results validation. Also, measurements from only the downward facing outgoing longwave radiation sensor, independent of the forcing data, were used to construct the assimilated skin temperature data set.

A separate meteorological series spanning 2004 from Wagga Wagga BoM data (Siriwardena et al., 2003), with rainfall data from the adjacent OzNet station (Smith et al., 2012; <http://www.oznet.org.au/k10.html>), was used as forcing for spinning up the model. The total rainfall used for the 2004 spin up and for the 2005 experiment periods are both close to the long term average of annual rainfall for the region, based on comparison with data from BoM records as shown in Table 1.

An actual evapotranspiration (ET) series was also derived for 2005 to provide a data set independent to the eddy covariance measurement series. This derived ET series was used for assessing LE predictions, as the assimilated heat flux observations were sampled from the eddy covariance series. The site specific data available to achieve this were rainfall—also used for model forcing—and root-zone (estimated to be within the top 60 cm for the grassland) soil moisture data consisting of both 0–30 cm and 30–60 cm deep probe measurements, which are

independent of the 0–8 cm measurements used for soil moisture assimilation.

This *ET* series was based on calculating differences between rainfall totals and root-zone soil moisture storage changes over time. It was calculated on a fortnightly time scale to minimise excessive noise in the series from moisture probe data, which is likely to be more prominent with respect to small moisture changes over shorter time scales. Potential *ET* calculated from meteorological data was used as an upper-bound for truncating any of the calculated actual *ET* that exceeded it. Of the twenty fortnightly *ET* totals that could be calculated from the available data, 35% of them clearly exceeded the corresponding potential *ET* and were hence reset to the potential value—all of these reset totals occurred consecutively in time spanning from the DoY 169 total through to DoY 302, in the austral winter and spring (mid-June to end of October). Deep drainage (below the 0–60 cm root-zone) and/or saturation excess surface runoff are the most likely reasons for the calculated *ET* exceeding its potential in this wetter/cooler period of the year when soil moisture was high. The total for DoY 316 immediately following this period exceeded the potential *ET* by a negligible amount (57.8 mm compared to 57.4 mm).

Outside the period from the DoY 169 total to DoY 316, where calculated *ET* exceeded potential *ET*, all of the fortnightly totals were considerably below potential. Within one of the driest periods of the year (late autumn) the calculated *ET* for the fortnight ending at DoY 141 was -4.1 mm. This negative value is attributed to soil moisture probe measurement errors in the dry conditions. Over the 60 cm measurement depth, 4.1 mm of water represents approximately 0.007 vol/vol moisture content, which is well within the moisture probe data error of ~ 0.02 vol/vol. Any *ET* occurring in the fortnight ending DoY 141 is therefore likely to be at or near the minimum for the year and close to zero.

This *ET* series provides for validation, enabling comparisons to be made between *ET* determined in two independent ways using the same rainfall data—from a complex model (CBM prediction with and without assimilation) and calculated from direct field measurements of soil moisture storage (supplemented with potential *ET* where appropriate). A regression between fortnightly rainfall and the calculated *ET* resulted in an R^2 of 0.07, indicating that the storage processes in the soil largely remove any dependence of the calculated *ET* on rainfall at a fortnightly time step. In constructing this series there was an assumption that, outside the period where calculated *ET* was limited to potential *ET*, there was no surface run-off over unsaturated soil in the pasture field where measurements were made.

From the station site there was no visually discernible gradient for at least a few hundred metres surrounding it. Where calculated *ET* totals were below potential, the near-surface and root-zone moisture were below saturation and 30 minute rainfall intensities (maximum observed was 8.4 mm in 30 min) were less than the estimated saturated hydraulic conductivity (Table 1), which equates to a 30 minute total of 15 mm. The hydraulic conductivity estimate comes from regional soil data analysis by McKenzie et al. (2003, 2000). Hence all of the rainfall for these periods is likely to have infiltrated into the soil.

The period of high root-zone soil moisture storage in the experimental year spans most of winter and spring with the main increase towards maximum storage beginning in June from \sim DoY 160. By \sim DoY 190 the storage approaches its maximum, and moisture content levels persist close to field capacity through to \sim DoY 290 in mid-October, sometimes peaking near saturation (values for these properties are in Table 1 and their origin discussed later in this section). The highest root-zone storage occurs within the period where potential *ET* dominates the constructed *ET* validation series, with rainfall that exceeded the potential assumed to have been balanced by percolation below the 60 cm root-zone depth and/or run-off. The 60–90 cm soil moisture probe data—which were not used for modelling or quantitative validation in this study—shows no notable change in moisture content below the root-zone from the beginning of the year until \sim DoY 200.

Possible groundwater interaction at the site is evident in the form of three separate extreme spikes in the 60–90 cm moisture data series that correspond with flow events (Table 2) in Kyeamba Creek at Book Book and Ladysmith (Fig. 1). This is indicative of lateral recharge of groundwater, followed by discharge (i.e. bank storage processes), related to flow events in Kyeamba Creek located ~ 350 m to the west of the study site. There are no independent measurements to verify the peak values of these moisture data spikes (up to and above ~ 0.55 vol/vol) which have only been interpreted qualitatively as indicators of groundwater influence, and while root-zone soil moisture data show some increases at these times they are not similarly extreme.

Groundwater interaction could have implications for the fortnightly *ET* validation series, particularly following the final 60–90 cm moisture data spike shown in Table 2 (DoY 311) leading into the spring/summer transition—the few days after this and beyond is where *ET* calculated from changes in root-zone moisture storage were maintained in the final data series as they were either equal to or less than the potential *ET*. In this period there might have been a small groundwater contribution to *ET* via capillary rise into the root-zone, which would be captured in the total *ET* of the validation series via soil moisture data, but which could not be quantified separately to it.

Soil parameters used in the CBM (see Table 1) were determined from a combination of samples collected at the site as part of this study, and soil property interpretations (McKenzie et al., 2000, 2003) relating to a 1:100,000 scale soil landscape map of the region (Chen & McKane, 1997). Particle size analysis performed on site samples determined that the top 60 cm of soil is fairly uniform and predominantly silty loam with clay and sand contents of $\sim 12\%$ and $\sim 33\%$ respectively (CSIRO particle analysis, May, 2007). A-horizon values from the map related soil interpretations (McKenzie et al., 2003) were used for wilting point (assumed to be the moisture content at 15 bar), field capacity (assumed to be the moisture content at 0.1 bar) and saturated hydraulic conductivity. Bulk density and porosity were determined using volumetric soil samples taken from the top 60 cm at the site, and together with the map related values for wilting point and field capacity, soil suction at saturation and the Campbell's *b* parameter were calculated.

Vegetation canopy height and the percentage of roots in each model soil layer were estimated from field observations. Leaf Area Index (*LAI*) values used for the site were monthly averages derived from 0.01° resolution Advanced Very High Resolution Radiometer (AVHRR) fPAR (Photosynthetically Active Radiation) data of Donohue et al. (2008). The fPAR data were converted through a fractional cover estimate (fPAR/0.95; see Lu et al., 2003) from which *LAI* was estimated (Choudhury, 1989). Values of *LAI* from such estimates are known to become less reliable when they are greater than ~ 3.0 (Carlson & Ripley, 1997; Lu et al., 2003). Moreover, McVicar et al. (1996) found that more than 90% of field sampled *LAI* values from a similar pasture environment in south east Australia were below 3.0. Therefore, any of the *LAI* estimates made for this site greater than 3.0 (for August through to November) were set to 3.0. Other parameter values used were provided with the CBM/CABLE model (default values; see Abramowitz, 2006) pertaining to the agricultural/C3-grassland category from a global vegetation dataset based on Potter et al. (1993).

4. Methodology

A one-dimensional CBM set-up was used following Pipunic et al. (2008) but with real field observations from point scale in-situ measurements, approximately representing overpass times of remotely sensed product types that can be derived from MODIS and AMSR-E observations. The grassland site where observations were made represents a land-cover for which remotely sensed microwave and thermal infra-red measurements are typically reliable. CBM simulations were performed using fixed parameters (derived from site specific information where possible or from regional datasets as outlined at the end of the previous section) and with the model uncalibrated, as

Table 2
Summary of major spikes in soil moisture data for below the root-zone (60–90 cm) corresponding to spikes in Kyeamba Creek discharge both upstream and downstream from the point in the creek closest to the study site.

Data set	Period 1 60–90 cm soil moisture spike			Period 2 60–90 cm soil moisture spike			Period 3 60–90 cm soil moisture spike		
	Increase to peak	Days at peak	Consecutive days rain total to peak	Increase to peak	Days at peak	Consecutive days rain total to peak	Increase to peak	Days at peak	Consecutive days rain total to peak
	60–90 cm soil moisture at flux station	DoY 252–253 0.26–0.63 vol/vol (~110 mm)	9	DoY 252–253 ~56 mm	DoY 270–272 0.29–0.57 vol/vol (~80 mm)	Data Gap	DoY 269–272 ~40 mm	DoY 310–311 0.19–0.55 vol/vol (~110 mm)	1
Discharge at Ladysmith (~14 km Upstream)	DoY 251–253 17–5588 Ml/day	1	–	DoY 270–272 77–2046 Ml/day	1	–	DoY 310–311 38–1106 Ml/day	1	–
Discharge at Book Book (~4 km Downstream)	DoY 251–253 11–1754 Ml/day	1	–	DoY 270–271 32–937 Ml/day	1	–	DoY 310–311 23–291 Ml/day	1	–

is the case with the current LSM in Australia's NWP system (Dr P Steinle, pers comm., May 2011).

Numerical experiments performed for this study included model simulations for 2005 with: i) no assimilation (denoted as “Open-Loop”); ii) *LE* and *H* observations assimilated together (denoted as “LEH_Assim”); iii) near-surface soil moisture observations assimilated (denoted as “SM_Assim”); iv) skin temperature—derived from observed outgoing longwave radiation—assimilated (denoted as “Tsk_Assim”); v) a combination of all observations assimilated—*LE*, *H*, near-surface soil moisture and skin temperature (denoted as “ALL_Assim”); and, vi) a combination of near-surface soil moisture and skin temperature assimilated (denoted as “SMTsk_Assim”). Available field observations of soil moisture and soil temperature, along with the calculated fortnightly *ET* estimates, were the independent data used for comparing with simulation outputs and assessing the impact of each assimilation option on predicted flux and state values.

Initial state conditions used for all the simulations were obtained from spinning up the CBM through repeated simulation using the one year meteorological forcing data series for 2004. The spin up was carried out until differences between model state values of soil moisture and temperature for the start of the year matched those at the end of the year for all soil layers to within 0.001 vol/vol and 0.01 °C respectively. This took 12 iterations, with most of this time attributable to minimising the differences for the deeper soil layers. CBM simulation time steps are governed by the time scale of forcing data and are therefore 30 min in this study.

In implementing the EnKF data assimilation algorithm, error estimates of field measurements were used to define the uncertainty range for generating observation ensembles, and these are summarised in Table 3. Model uncertainty for the EnKF is defined from the spread of an ensemble of model predictions, which in this study was the result of performing simulations with ensembles of key model inputs. Specifically, these were ensembles of initial state conditions and forcing data variables that represented error range estimates of each, since these inputs contribute to overall model error. Inaccurate model structure and parameterisation are also major sources of model error, which due to their complexity are very difficult to represent with ensembles. Hence they have not been treated directly in the ensemble generation for this study. Ensemble generation is discussed later.

In all simulations for numerical experiments spanning 2005, ensembles of model inputs included perturbed 2005 forcing data (Table 4) and perturbed initial state conditions, with covariance inflation applied

to model state ensembles just prior to state update calculations. Fixed values of key parameters are included in Table 1. More detail on perturbing model inputs and states for ensemble generation follows. The ensemble mean of each simulation is taken as the modelled estimate of the truth.

4.1. Assimilation observations

The field observations used for assimilation were sub-sampled from the original one-dimensional observation data sets, guided by daytime satellite overpass times of MODIS and the night-time overpass time of AMSR-E; while AMSR-E recently ceased operation its successor AMSR2 is expected to provide similar data (Imaoka et al., 2010). Other studies where the focus incorporated the Kyeamba Creek region found that AMSR-E soil moisture produced from local night-time overpass data was of superior quality to that from daytime data (Draper et al., 2009b; Su et al., 2013). Hence the soil moisture data were sampled daily at 2 am local time, approximating the night-time AMSR-E overpass, while it is acknowledged that AMSR-E data would not always be available every day for this site.

Thermal infra-red related observations—*LE*, *H* and skin temperature—were sampled twice daily at 10 am and 2 pm local time to represent data available from MODIS for daytime when *ET* is most active. Sampling skin temperature for assimilation on the same time steps as *LE* and *H* provides an important insight into the relative merits of assimilating these different data types, given that the derivation of instantaneous remotely sensed *LE* and *H* uses remotely sensed skin temperature. While these data can also be derived at hourly (MTSAT1R) and bi-weekly (Landsat TM) timescales, only the MODIS timescale is explored here. Pipunic et al. (2008) explored the assimilation of bi-weekly *LE*, *H* and skin temperature and found that they resulted in much poorer results than for MODIS intervals. Since clouds can obscure remotely sensed TIR data, which relate to skin temperature and hence also *LE* and *H* observations, further sub-sampling of these observations at MODIS overpass times was performed for cloud free conditions (defined here as where incoming solar radiation for the site was greater than 90% of expected clear sky radiation for the day). Cloud screening for real MODIS data would likely involve greater complexity and uncertainty, especially with partial cloud cover, compared to the procedure using in-situ ground data adopted here. The frequency of assimilated observations is displayed on plots of simulation results in Figs. 2 through 4.

Table 3
In-situ observations of remotely sensed data types used in this study, with estimated additive error ranges used for ensemble σ values, and satellite sensor information that each observation represents.

Observed quantity	Additive error (ensemble σ)	Corresponding satellite/sensor	Temporal resolution used	Spatial resolution available
LE (Wm^{-2})	± 50	MODIS	Twice daily, filtered for cloud	~1 km \times 1 km
H (Wm^{-2})	± 50	MODIS	Twice daily, filtered for cloud	~1 km \times 1 km
Near-surface soil moisture (vol/vol)	± 0.04	AMSR-E	Once per day (am)	~25 km \times 25 km
Skin temperature (K)	± 2	MODIS	Twice daily, filtered for cloud	~1 km \times 1 km

Table 4

Meteorological forcing variables perturbed for ensemble generation. Comparisons between Kyeamba Creek and Wagga Wagga BoM point measurements assisted with estimating the σ (as per Turner et al., 2008) for ensemble generation.

Forcing variable	Estimated σ for ensembles
Short-wave in	~15%
Long-wave in	~35Wm ⁻²
Precipitation	~60%
Air temperature	~2 °C
Wind speed	~45%
Specific humidity	~0.0007 kg/kg

The root mean square error between eddy covariance *LE* and *H* data before and after closing the energy balance is ~40 Wm⁻² each. A review of derivation methods for TIR based remotely sensed heat fluxes by Kalma et al. (2008) found the average root mean square error for such data to be ~50 Wm⁻² based on a survey of validation studies. Consequently, this value was used here for the assimilated *LE* and *H* uncertainty. For soil moisture, a value of 0.04 vol/vol was used. While in-situ calibration results indicated an uncertainty of ~0.02 vol/vol, this was increased for consistency with errors in satellite derived observations for a similar Australian environment (Draper et al., 2009b). As direct TIR data were not available, skin temperature observations were derived using measured outgoing longwave radiation by solving for the temperature term in the Stefan–Boltzmann equation using an assumed emissivity of 0.98 (Wan & Dozier, 1996). The uncertainty range used for these observations was 2 K, based on some error range estimates for remotely sensed skin temperature quoted in literature (e.g. Kaleita & Kumar, 2000; Sun et al., 2004; Wang & Liang, 2009).

The shallowest volumetric soil moisture measurements made were 0–8 cm and consequently these were the observations assimilated. They correspond exactly with the depth averaged values over the top two CBM soil layers (2.2 and 5.8 cm respectively) but exceed the observation depth of real AMSR-E soil moisture data (~1–2 cm), which might have implications for appropriately representing remotely sensed data assimilation.

In a synthetic study by Walker et al. (2001b) the depth of assimilated soil moisture data had no significant influence on the time taken to retrieve the deeper root-zone moisture profile, although the authors note that the ability to impact the deeper moisture profile from assimilating near-surface observations depends on the correlation between soil moisture states over depth. A more detailed synthetic study by Kumar et al. (2009) spanning multiple years, and using multiple LSMs with different subsurface physics and soil layer depths, found that when the coupling between the surface and root-zone is stronger the benefit of assimilating near-surface soil moisture observations to improve root-zone prediction is higher.

To the authors' knowledge, no studies using real data for a broad range of observation depths exist in the literature, thus it is not clear to what extent the measurement depth can influence root-zone impacts in real systems. The possibility exists that the 0–8 cm near-surface soil moisture used here might sometimes have a stronger correlation with the root-zone compared to the top ~1–2 cm, and thus its assimilation may also have an overstated impact on the root-zone compared to assimilating data for the shallower AMSR-E product depth. It was not possible to investigate this issue here as the 0–8 cm measurements were the shallowest available, hence why only satellite overpass repeat intervals were considered in relation to representing remotely sensed moisture data.

4.2. Observation-model bias removal

Prior to assimilation, the in-situ near-surface soil moisture used for assimilation was rescaled, to eliminate systematic differences relative to the CBM predicted near-surface soil moisture series from

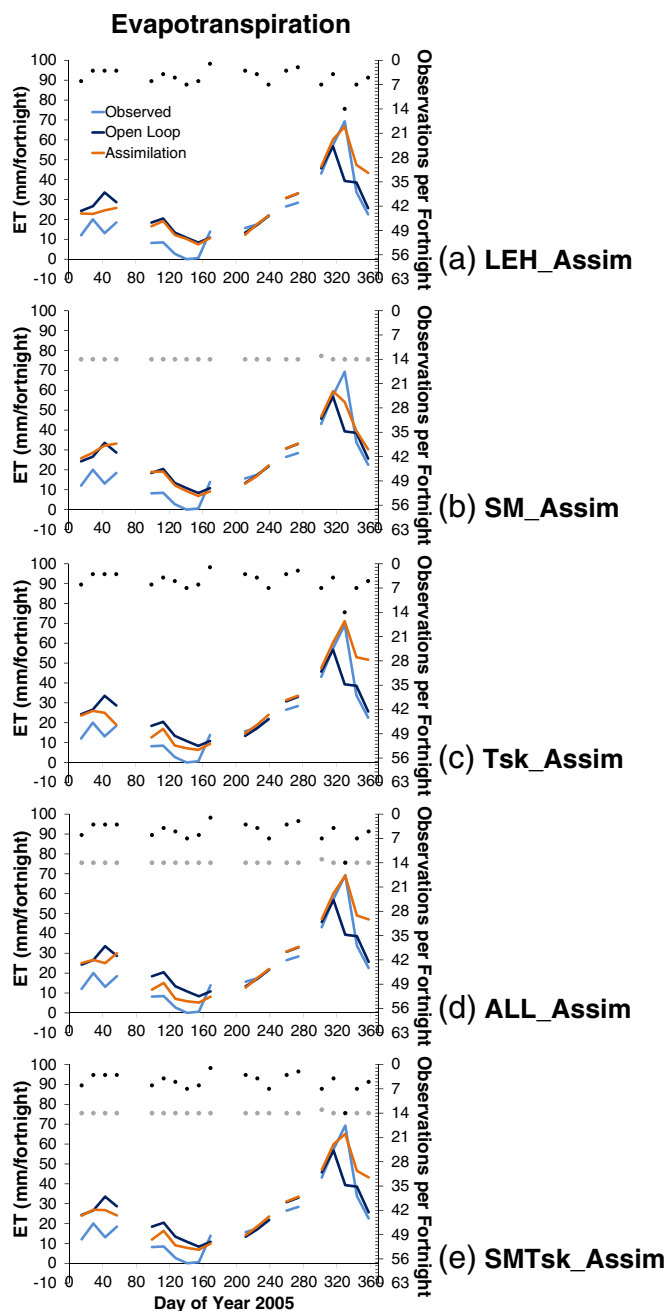


Fig. 2. Plots of fortnightly ET totals for Kyeamba Creek showing: Observed validation series, Open-Loop simulations, and from top to bottom the assimilation experiment outputs from a) LEH_Assim; b) SM_Assim; c) Tsk_Assim; d) ALL_Assim; and, e) SMTsk_Assim. Dots along the top of each plot correspond to the assimilation frequency (right hand axis) for LE, H and skin temperature observations (black), and soil moisture observations (grey).

Open-Loop, both in terms of its annual mean and its standard deviation. For skin temperature there was no significant difference in terms of the mean and standard deviation between observations and comparable Open-Loop predictions (based on an F-Test for variances followed by a t-Test for means assuming equal variances) hence this data series was not rescaled. The soil moisture rescaling was applied using:

$$\theta'_{Obs} = (\theta_{Obs} - \mu(\theta_{Obs})) \times \left(\frac{\sigma(\theta_{CBM})}{\sigma(\theta_{Obs})} \right) + \mu(\theta_{CBM}) \quad (2)$$

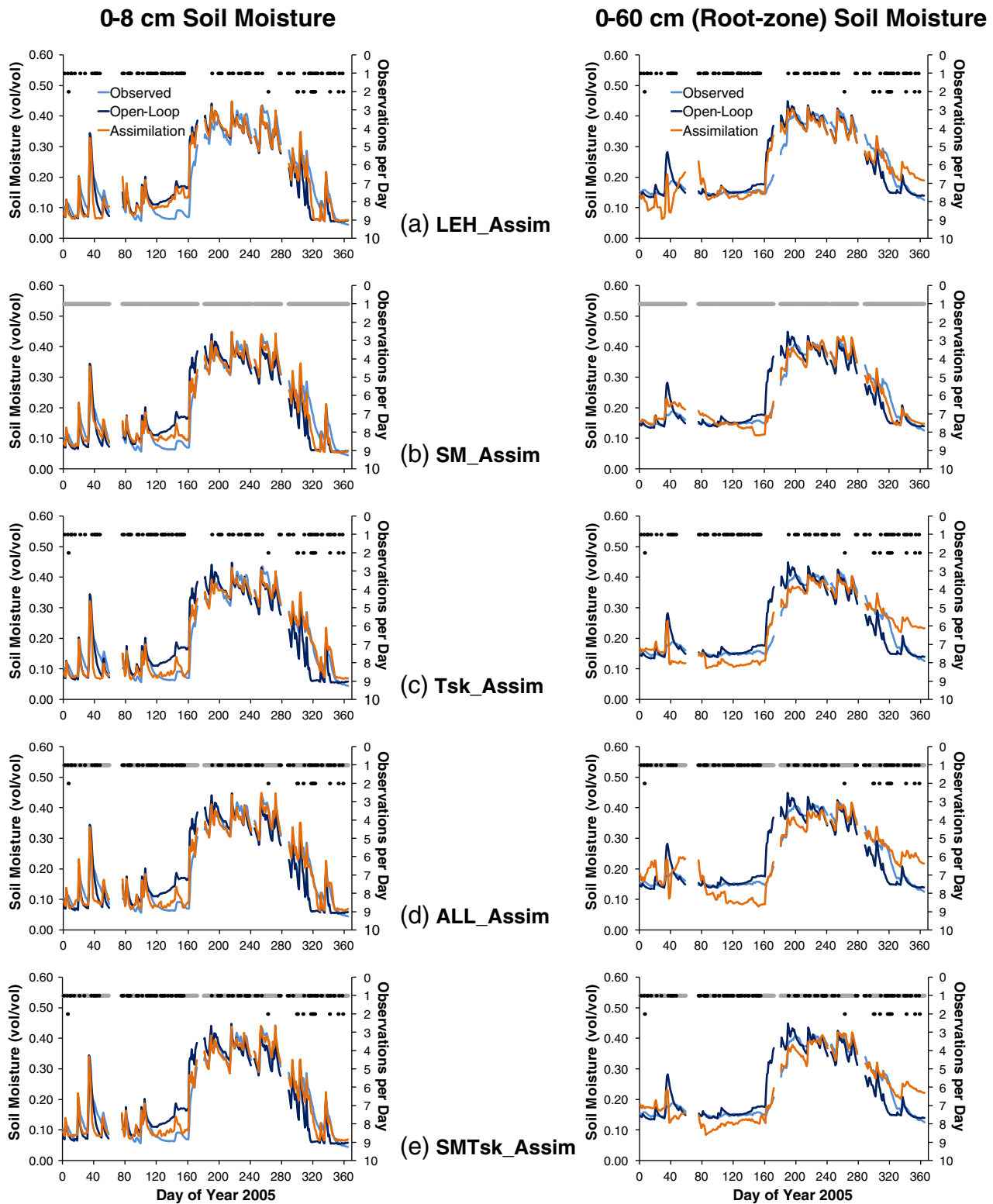


Fig. 3. Plots of daily averaged (midnight to midnight) soil moisture for Kyeamba Creek showing: Observed validation series, rescaled Open-Loop simulations and in each row the rescaled assimilation experiment outputs from a) LEH_Assim; b) SM_Assim; c) Tsk_Assim; d) ALL_Assim; and, e) SMTsk_Assim. Dots along the top of each plot correspond to the assimilation frequency (right hand axis) for LE, H and skin temperature observations (black), and soil moisture observations (grey).

where the rescaled near-surface soil moisture observations θ'_{Obs} used for assimilation were calculated using the mean ($\mu()$) and standard deviation ($\sigma()$) of the 0–8 cm observed series (θ_{Obs}), and of the series of CBM Open-Loop moisture predictions depth averaged over 0–8 cm (θ_{CBM}) for coincident time steps in the experiment period.

4.3. Assimilation implementation and assessment

Different ensemble sizes were tested with the EnKF and 20 ensemble members were found to be sufficient for use with the CBM, congruent with earlier findings from the synthetic-twin study by

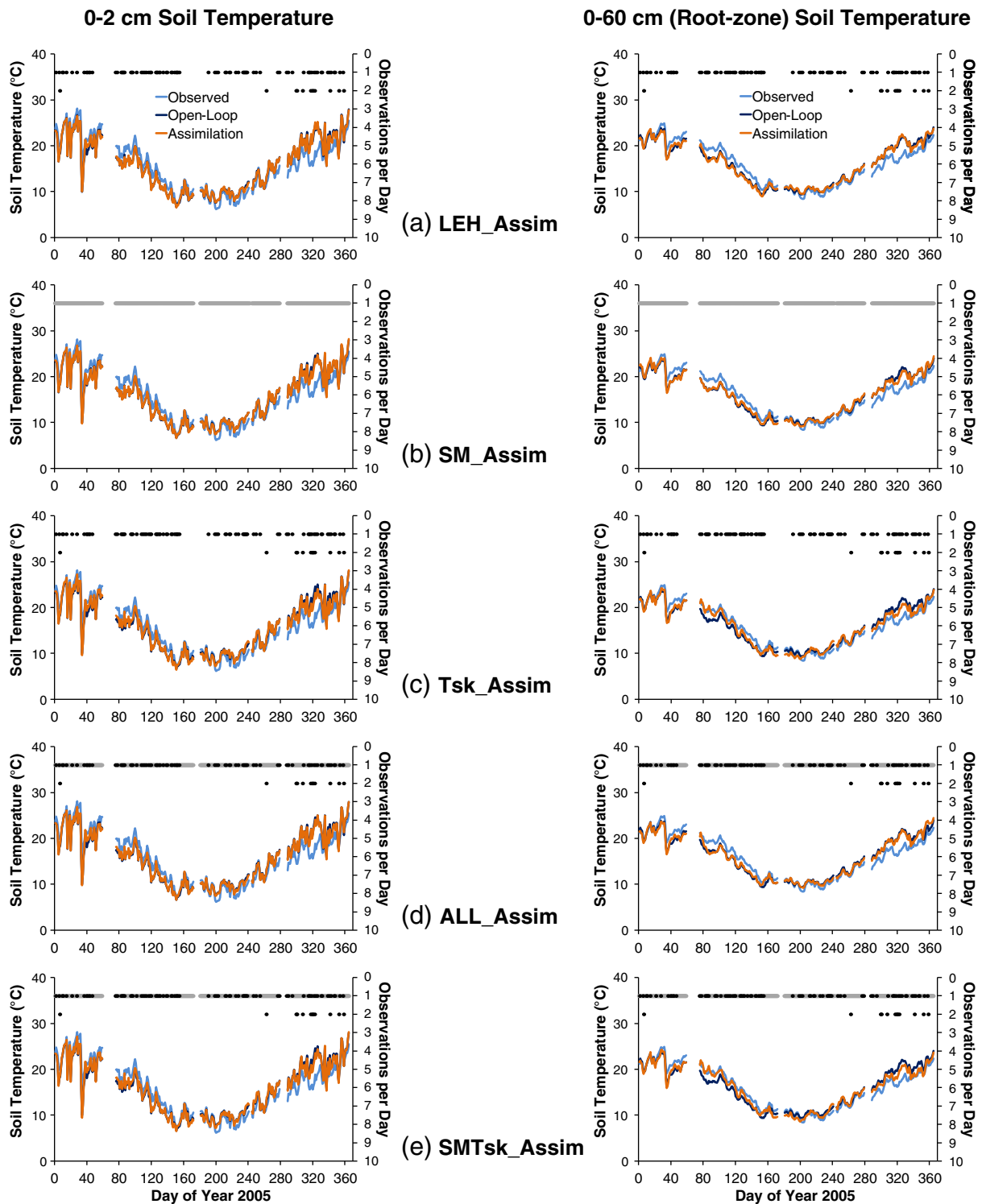


Fig. 4. Plots of daily averaged (midnight to midnight) soil temperature for Kyeemba Creek showing: Observed validation series, rescaled Open-Loop simulations and in each row the rescaled assimilation experiment outputs from a) LEH_Assim; b) SM_Assim; c) Tsk_Assim; d) ALL_Assim; and, e) SMTsk_Assim. Dots along the top of each plot correspond to the assimilation frequency (right hand axis) for LE, H and skin temperature observations (black), and soil moisture observations (grey).

Pipunic et al. (2008). Ensemble generation involved adding random perturbations to model initial conditions and forcing data, and to observations as ensembles of observations were assimilated. Perturbations were derived from random numbers generated with a normal distribution around a mean (μ) of zero with a standard deviation (σ) equal to the estimate of the error standard deviation of the particular data being perturbed. Ensembles were produced such that members were

spread within the 95% confidence interval (C.I.) as determined from the assumed data uncertainty.

For observations (treated as ensemble means), the σ values were based on the estimates of observational uncertainties in Table 3. Ensembles of initial model state conditions were generated from the spun-up initial soil moisture and temperature values. While initial state perturbations do not persist in contributing to long-term

ensemble error representation (unlike forcing perturbations which apply throughout a simulation time series) they were used for initiating the ensemble spread with values of $\sigma = 0.03$ vol/vol selected here for perturbing initial soil moisture and $\sigma = 3$ °C for perturbing initial soil temperature in each layer. The approach of Turner et al. (2008) was used as a guide for generating meteorological forcing ensembles, which factors in measurement error and representative errors when using forcing data from multiple point locations. Both flux station site forcing data and data from the ~20 km distant Wagga Wagga BoM station (for gap filling) were used here—discrepancies between the full 2005 series of these two datasets were used to estimate representative error for each variable (based on Turner et al., 2008). The approximate errors relating to ensemble generation are included in Table 4.

Given that model structural error or parameter uncertainty were not specifically accounted for in the ensemble generation, and with the potential for filter divergence to affect EnKF performance over time, covariance inflation (e.g. Anderson & Anderson, 1999) was applied prior to updating at assimilation times. It was applied by adding small perturbations to each state ensemble member to slightly increase the spread about the mean prediction. For the CBM near-surface soil layer (2.2 cm thick), soil moisture ensemble members were inflated by adding random perturbations generated with $\sigma = 0.01$ vol/vol, while $\sigma = 1$ °C was used for soil temperature. These σ values ensured a small inflation of ensemble spreads to increase the likelihood that state error quantities associated with unknown parameter and model structure errors are factored in at update times. For additive inflation of subsequent deeper soil layer ensembles, σ values were scaled down fractions of the values used for the surface layer, with the scaling based on the ratio between the surface layer thickness and each subsequent layer's thickness. This was to account for the expectation that random state errors are dampened with the deeper/thicker soil layers, which has implications for state error correlations between layers, and hence EnKF error covariances and filter performance. The use of covariance inflation and basic assumptions about error correlations are employed here in the absence of a complete understanding of all errors that would enable optimal depictions of them with predicted ensembles. A detailed investigation for understanding all aspects of model error is a major task beyond the scope of this study.

Assessments of the model simulations were made by comparing predictions with independent field data for the variables of interest—*ET*, root-zone soil moisture, and surface and root-zone soil temperature. Root Mean Squared Error (RMSE) and Nash Sutcliffe coefficient of efficiency (E) metrics for quantifying magnitudes of error, and the coefficient of determination (R^2) for quantifying the goodness of fit in terms of variance, were used to assess simulation predictions against the independent field data. Prior to these assessments, state variable predictions from all simulations (Open-Loop and assimilation experiments) were rescaled so that their mean and standard deviation matched that of the corresponding time series of independent field observed states used for comparison (by substituting relevant values into Eq. (2)). This ensured that the subsequent state comparisons were bias free relative to the best available representation of the true states as observed with in-situ soil temperature probes and soil moisture probes that were calibrated for the site.

Soil moisture comparisons were made for two different depths, including the near-surface (0–8 cm) representing the depth of the assimilated soil moisture observations (as a sanity check) and the deeper 0–60 cm profile (an average of 0–30 cm and 30–60 cm field observations) corresponding to the estimated vegetation root-zone. For soil temperature, comparisons were made between the shallowest observation (2 cm) and the top soil layer in the model (0–2.2 cm), being the prognostic temperature variable linked to the *LE* and *H* soil component calculations. A weighted average of soil temperature measurements throughout the soil profile was used for comparison with the model root-zone (0–60 cm) prediction.

5. Results

Fortnightly totals of *ET* were calculated from 30 minute simulation outputs in order to compare with the independent *ET* series that was derived directly from field observed data. Therefore a fortnightly scale was the smallest time unit for which *ET* comparisons were made. It is acknowledged that for NWP the diurnal surface heating is very important and hence comparisons for the full series of 30 minute heat flux predictions would be informative. However, it was not possible to make independent comparisons at a 30 minute time step here, given the available validation data. Comparisons for soil moisture and soil temperature were both made using daily averaged (midnight to midnight) values from the 30 minute observed and simulated series. Rescaling the simulated series of these states to match the observations was applied to the daily averages prior to any comparisons.

Figs. 2 to 4 are time series plots showing observed site data together with simulation predictions and the frequency of assimilated observations included across the upper horizontal axis. Each vertical sequence of five plots in the figures shows simulation results from a separate assimilation experiment. Qualitative descriptions comparing simulated and observed time series based on these plots are presented in following sub-sections. Quantitative comparisons for all experiments in the form of RMSE, E and R^2 values between observed and simulated values are provided in Table 5. These scores were calculated using the data on the same time scales on which they are plotted in Figs. 2 to 4 and highlight the best performing simulation(s) overall relative to observed validation data. Fig. 5 shows the changes made by each experiment in terms of RMSE between observations and predictions relative to RMSE between Open-Loop predictions and observations.

5.1. Open-Loop comparisons

5.1.1. Open-Loop *ET* output

Differences between predicted *ET* from Open-Loop and the estimates from observations vary across the experiment year (Fig. 2). From the austral summer at the start of the year through to early winter at around DoY 160, the observation derived *ET* was over-predicted by as much as ~20 mm/fortnight (~DoY 40). Therefore, possibly too much of the rainfall in this period became *ET* via the model, presumably due to inaccurate soil and vegetation parameters and/or physical processes in the model, and hence incorrect soil moisture (in both the near-surface and root-zone – Fig. 3). As noted in Section 3 the observed 60–90 cm moisture series, beneath the root-zone as defined here, is static throughout this period ruling out any groundwater contribution. Another contributing factor may be that time invariant root distribution in the model over-states the amount of water drawn for transpiration from deeper soil in periods where grass is shorter and its growth is sparse around the site (especially where Open-Loop root-zone moisture is over-estimated). The vegetation cover in this period from the beginning of the year to ~DoY 160 is minimal where *LAI* values range from 0.39 to 0.85 with a mean of 0.53.

Through the winter and most of spring (from DoY 160 to 316) where most of the observation based *ET* values were set to the calculated potential *ET*, in what is predominantly an energy limited period with relatively high moisture storage in the soil profile for the year, Open-Loop *ET* predictions track the observation series closely with the only noticeable difference being negligible over-predictions of ~5 mm/fortnight occurring for the ~DoY 260 and 274 totals. This close match is not surprising given that with high water availability in the soil profile the CBM is expected to predict *ET* close to the potential rate.

After DoY 316 to the end of the year (most of November through December) is where the largest discrepancies occur, with observed *ET* under-predicted by Open-Loop by as much as 30 mm/fortnight. This period is characterised by warming where the high soil moisture storage of winter/spring transitions to a water limited scenario with increased incoming radiation, and where high vegetation cover for

November (*LAI* of 3.0) declined in December (*LAI* of 1.21). As discussed in Section 3 there is evidence indicating possible groundwater interaction around DoY 311 (refer to Table 2). Thus any water added to the soil profile as a result could have contributed to root-zone water availability for *ET* over the following days or weeks. This may explain the large under-prediction of *ET* by Open-Loop after DoY 316, as the only water supply information available for CBM calculations was from rain-fall forcing data.

5.1.2. Open-Loop soil moisture output

Plots in Fig. 3 also show variation in differences between Open-Loop soil moisture predictions and observations throughout the experimental period. Early in the year through summer and autumn (to ~DoY 120), the depletion of Open-Loop soil moisture compared to observations for the near-surface assimilation depth (0–8 cm) is from higher peak values and up to twice as fast in parts, particularly in early February (~DoY 35–40) where the peak is over-estimated by ~0.09 vol/vol. Following on, between ~DoY 120 and 160, the observations indicate a mostly dry period where they are increasingly over-estimated. Much of these discrepancies from the beginning of the year to ~DoY 160 are consistent with Open-Loop over-estimating *ET* in this period. The response of the Open-Loop near-surface soil moisture at ~DoY 160 in June to the beginning of the major increase in winter/spring moisture storage is accurately timed, with some over-estimation persisting through the first half of this period. In the spring/summer dry-down period there is another large discrepancy, with the Open-Loop under-estimating observations by as much as ~0.15 vol/vol, which is again consistent with the *ET* under-estimation in this period (Fig. 2).

Deeper root-zone (0–60 cm) soil moisture content from Open-Loop shows a similar relationship in terms of variation with respect to observations as for the near-surface moisture plots, albeit with the magnitude of variations being less pronounced. In particular, the over-estimation and more rapid depletion of root-zone moisture compared to observations for instances in the first ~100 days and under-estimation around ~DoY 320–330 (Fig. 3) are consistent with the respective over-estimation and under-estimation of *ET* for periods incorporating these times (Fig. 2). As noted in relation to *ET* predictions, inaccurate model parameters could have contributed to discrepancies between Open-Loop predictions and observations here, while the inability to prescribe different soil parameters with depth for different model layers might also be a contributing factor.

5.1.3. Open-Loop soil temperature output

Surface soil temperature plots (0–2 cm) in Fig. 4 show a general pattern of Open-Loop predictions under-estimating observations in the drier austral summer/autumn period up to ~DoY 150. Then across the first half of winter from June to mid-July (~DoY 150–200) which includes some of the coolest temperatures of the year the Open-Loop tracks the observations very closely. From mid-winter until the end of the year as the temperature increases, predictions mainly over-estimated the observations with the largest differences (up to 6 °C) occurring in November between ~DoY 310–330—the period in which Open-Loop soil moisture and *ET* predictions under-estimated their respective observations by

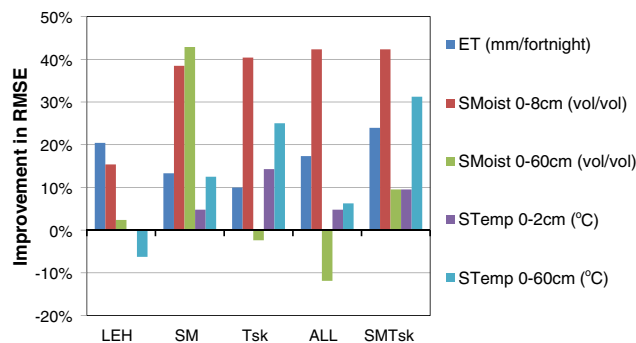


Fig. 5. Comparative improvements over Open-Loop made by each assimilation experiment in terms of RMSE reduction for heat flux and soil state predictions.

relatively large magnitudes (Figs. 2 and 3) and where groundwater interaction is a possibility (Table 2).

As with soil moisture, the deeper 0–60 cm root-zone soil temperature predictions from Open-Loop exhibit a similar pattern of discrepancy with observations as for the near-surface soil temperature. The main difference being the root-zone series has less day-to-day variation, as expected, and the differences with observations are sometimes slightly less in magnitude than the corresponding differences for near-surface soil temperature.

5.2. Assimilation comparisons

5.2.1. Assimilation *ET* output

From the beginning of the year up to early winter at ~DoY 160, where Open-Loop *ET* predictions over-estimate observations (Fig. 2), the best overall improvements to *ET* were from simulations where the assimilation involved skin temperature observations and combinations of variables (i.e. Tsk_Assim, ALL_Assim and SMTsk_Assim). The only notable impact from LEH_Assim here was in the summer with some improvement within the first ~60 days. When only soil moisture was assimilated (i.e. SM_Assim), no notable impact or improvement was made to *ET* estimates for this entire period.

Through the mainly energy limited period with increased moisture availability that covers most of winter/spring (between ~DoY 160 and 316), where observed and Open-Loop *ET* series are at or near potential *ET* with no notable differences between them, the predictions from every experiment were maintained at approximate potential *ET* values. While each assimilation experiment made clear improvements to *ET* in the period between DoY 316 and ~DoY 330–340, where Open-Loop under-estimated the observed series most. All of the experiments except for SM_Assim resulted in very close matches to the maximum observed *ET* at ~DoY 330 although unlike SM_Assim they caused over-estimation from ~DoY 340 onwards where Open-Loop and observations were relatively close.

5.2.2. Assimilation soil moisture output

From the beginning of the year through to ~DoY 160, being before the major winter/spring moisture storage period, predictions of

Table 5

Statistics for comparisons between simulations (rows) and independent observations over the 2005 experiment period, calculated after removing biases for state variables. Bold values indicate most improvement to simulated values of interest (columns).

	ET (mm/fortnight)			SM 0–8 cm (vol/vol)			SM 0–60 cm (vol/vol)			ST 0–2 cm (°C)			ST 0–60 cm (°C)		
	R ²	RMSE	E	R ²	RMSE	E	R ²	RMSE	E	R ²	RMSE	E	R ²	RMSE	E
Open-Loop	0.71	10.8	0.63	0.83	0.052	0.82	0.84	0.042	0.83	0.86	2.1	0.86	0.88	1.6	0.88
LEH_Assim	0.88	8.6	0.76	0.88	0.044	0.87	0.85	0.041	0.84	0.86	2.1	0.86	0.87	1.7	0.86
SM_Assim	0.83	9.4	0.72	0.94	0.032	0.93	0.95	0.024	0.95	0.87	2.0	0.87	0.90	1.4	0.90
Tsk_Assim	0.85	9.8	0.70	0.94	0.031	0.94	0.83	0.043	0.82	0.89	1.8	0.89	0.93	1.2	0.93
ALL_Assim	0.87	9.0	0.75	0.94	0.030	0.94	0.80	0.047	0.79	0.88	2.0	0.88	0.89	1.5	0.89
SMTsk_Assim	0.89	8.2	0.78	0.94	0.030	0.94	0.87	0.038	0.87	0.89	1.9	0.88	0.94	1.1	0.94

near-surface soil moisture (0–8 cm) were improved overall by each data assimilation approach compared with Open-Loop. SM_Assim improvements were the most consistent (Fig. 3) while for other approaches where either skin temperature or *LE* and *H* observations were involved in the assimilation, soil moisture was slightly degraded by over-correction at ~DoY 40–50 during the dry-down after high rainfall. Improvements to near-surface soil moisture were also made by each simulation over the remainder of the year after ~DoY 160, with simulations involving skin temperature observations (i.e. Tsk_Assim, ALL_Assim and SMTsk_Assim) performing particularly well over the spring to summer dry-down period post ~DoY 310. The consistency of SM_Assim in making some improvement across all seasons of the experiment year in relation to near-surface moisture observations (the 0–8 cm series which assimilated observations were sampled from) instilled confidence in the assimilation scheme.

For root-zone soil moisture, SM_Assim produced the best overall improvement across the year. Predictions from the other simulations which involved skin temperature and/or heat flux observations in the assimilation were poorest and most degraded in drier periods within the first half of the year and at the end post ~DoY 320 (Fig. 3a, c, d and e). During the wetter winter/spring period these simulations performed reasonably well, improving parts of the root-zone moisture series and without any extreme degradation. In this period the moisture content was more uniform over the root-zone and near-surface moisture dynamics were more strongly correlated with dynamics through the root-zone depth.

A possible reason for the better and more stable results in the wetter period is that the ensemble generation might have produced more adequate error representations for predicted observations and predicted root-zone moisture states here. In which case the resulting EnKF error covariances would have been a good reflection of actual error correlations between these predictions, hence the more reasonable root-zone moisture state updates. Compared to wetter seasons, moisture dynamics were more weakly connected through the root-zone in drier periods where greater contrasts in moisture over depth occurred—e.g. such as wetter near-surface soil from isolated rain events compared to drier deeper soil. The degraded root-zone moisture in drier periods from most simulations may have been due to poorer error representations for these particular conditions, such that EnKF covariances did not adequately reflect error correlations between predictions of assimilated observations and the different root-zone soil moisture states.

5.2.3. Assimilation soil temperature output

Fig. 4 illustrates soil temperature outputs from all simulations for the CBM surface soil layer (0–2.2 cm) and root-zone (0–60 cm). The relevance of the surface soil layer temperature here is its use in the soil component of the CBM calculated total skin temperature (Eq. (1)), and also in the calculation of soil components of *LE* and *H*. Assimilation impacts on the surface soil layer temperature appear relatively minor across all of the simulations, and any impacts that were made are most noticeable for warmer periods, including from ~DoY 40 to 100 in the first half of the year and towards the end of the year from ~DoY 300 to 340 where the impact on *ET* was greatest from all assimilation approaches. The best improvements for these periods were from Tsk_Assim, which is expected due to the surface soil layer temperature being linked directly to skin temperature in the CBM.

For periods of high vegetation cover, such as the second half of the year (where LAI is 2.4 for July, 3.0 from August through November, and 1.2 for December), the direct impact on heat fluxes from any surface soil layer temperature state adjustments were minimal. The adjustments to *ET* at the end of the year (> ~DoY 316) from Tsk_Assim are assumed to be related to impacts on soil moisture (compare Figs. 2c and 3c). This is likely due to the vegetation canopy components of *LE* and *H* in the CBM dominating the total predicted values of *LE* and *H* in this period, where the vegetation canopy surface temperature used in the CBM vegetation

heat flux calculations (also for the vegetation component of skin temperature—see Eq. (1)) is based on the non-prognostic leaf temperature variable. Hence, for the LEH_Assim simulation there is very little impact on surface soil layer temperature for the period at the end of the year from ~DoY 316 onwards (Fig. 4a), which coincides with some of the greatest adjustments to *ET* predictions (Fig. 2a). While for ~DoY 40 where LEH_Assim had some noticeable impact on correcting surface soil layer temperature, coinciding with an adjustment to *ET*, there is minimal vegetation cover (LAI of 0.6) and therefore surface soil layer temperature values feature more prominently here in calculated *LE* and *H* totals from the CBM.

The experiments Tsk_Assim and SMTsk_Assim made the greatest changes/improvements to root-zone soil temperature predictions reinforcing that skin temperature observations are the main driver for soil temperature state impacts. From Fig. 4c and e, the greatest improvements were made in the first half of the year between ~DoY 80 and 160 where vegetation cover was low and the Open-Loop underestimated observations, and also towards the end of the year post ~DoY 280 incorporating the period where vegetation cover was highest and also where *ET* adjustments were greatest. LEH_Assim and SM_Assim had minimal overall impact on root-zone temperature across the year by comparison (Fig. 4a and b), with root-zone soil temperature generally lacking a strong relationship with heat fluxes, particularly as vegetation cover increases (in the second half of the year).

6. Discussion

Based on the results presented, the overall differences between simulations are summarised and interpreted here. From the R^2 and E scores for Open-Loop predictions (Table 5) the dynamics of the validation *ET* data series in this study were generally more difficult to simulate than near-surface and root-zone soil moisture and temperature observations. LEH_Assim was expected to produce amongst the best *ET* predictions given that state updates were driven only by heat flux observations. While it led to a strong reduction in RMSE of 20% compared to predictions from Open-Loop, the level of improvement trailed that made by SMTsk_Assim which reduced RMSE by 24% but was greater than improvements from ALL_Assim which reduced RMSE by 17%. The comparative improvements between these three simulations are supported by all of the metrics used. Although these were the top three performers for *ET* amongst all of the experiments, their impact on root-zone soil moisture predictions were varied, with ALL_Assim producing the most degraded results of all experiments, SMTsk_Assim making fairly solid improvements, and LEH_Assim making only minor overall improvement.

The relatively poor impact LEH_Assim had on state variables in contrast to strong *ET* improvements as per the quantitative scores highlights the challenge of simultaneously improving all state variables and heat fluxes given the inherent uncertainties associated with complex relationships between them in LSMs. Scores for SM_Assim and Tsk_Assim indicate they made amongst the greatest improvements to soil moisture and temperature state variables respectively along with SMTsk_Assim which performed well for both. This supports the expectation that assimilated observations will usually lead to strong improvements for the most directly related model variables.

Despite SM_Assim producing the best root-zone soil moisture with a reduction in RMSE of over 40%, the corresponding reduction in RMSE of 13% for *ET* indicates only a modest improvement relative to validation data compared with other experiments. When considered together with the top three experiments for *ET* improvement which had varied impacts on root-zone soil moisture, it is clear that specifically improving root-zone moisture will not necessarily optimise the heat flux predictions. Moreover, the inconsistency between quantitative soil temperature scores for SMTsk_Assim and LEH_Assim, which both strongly improved *ET*, and between the strong soil temperature and only modest *ET* improvements from

Tsk_Assim compared to those from LEH_Assim, supports the qualitative time series interpretations (discussed in the previous section) that improved soil temperature prediction does not always make a strong contribution to *ET* improvement throughout the whole year—particularly as vegetation cover increases.

Comparing the impacts on *ET* from LEH_Assim and from experiments using skin temperature and no heat flux observations is of particular interest when considered in a remote sensing context. LEH_Assim represented the assimilation of *LE* and *H* data which would first need to be derived from thermal and visible remote sensing imagery using an energy balance model separate to the LSM. However, remotely sensed skin temperature represented in Tsk_Assim and SMTsk_Assim is more directly available from the thermal imagery used in deriving *LE* and *H*. The results for *ET* prediction from both SMTsk and LEH_Assim (Table 5 and Fig. 5) indicate that there may be no significant benefit from assimilating remotely sensed *LE* and *H* over using skin temperature together with an observation directly related to the water balance (i.e. soil moisture) for improving heat flux prediction, especially when considering the additional modelling required to produce remotely sensed *LE* and *H*.

Quantitative results for the SMTsk_Assim experiment highlight some clear benefits of multi-observation assimilation. It produced the greatest improvements to *ET* relative to validation data of any experiment, presumably due to cumulative positive impacts from the different observations used, which when assimilated separately each improved *ET* to lesser degrees (through Tsk_Assim and SM_Assim experiments). The multi-observation approach of ALL_Assim also produced relatively strong *ET* improvements, but was inconsistent in terms of state variable improvements, with root-zone soil moisture having been degraded more than from any other experiment. This may be due to the combined impact of *LE*, *H* and skin temperature (which produced poor or degraded root-zone soil moisture via LEH_Assim and Tsk_Assim) outweighing any beneficial impacts from the soil moisture observations. The worst impacts on root-zone moisture from ALL_Assim were mainly for drier periods, which is congruent with the worst impacts from LEH_Assim and Tsk_Assim (compare Fig. 3a, c and d).

The SMTsk_Assim multi-observation approach and SM_Assim were the only simulations in this study which simultaneously improved predictions of all of the assessed variables against validation data (Table 5 and Fig. 5). This demonstrates that assimilating soil moisture and directly impacting the model water balance improved soil state variables and *ET*, while incorporating an additional observation type linked directly to model energy balance calculations (skin temperature) could still lead to improved state variables, and most importantly in the NWP context, also produce optimal *ET* predictions. The added benefit of SMTsk_Assim is of course the potential for good *ET* prediction while avoiding the intermediate modelling step to estimate *LE* and *H* from thermal and visible imagery when assimilating remotely sensed data.

The varying assimilation results during the year, and particularly the degradation caused by some of the assimilation scenarios, point to the likelihood of systematic model errors. As an example, the root distribution in CBM soil layers is represented by user prescribed parameter values which are time-invariant. With a seasonally varying vegetation cover (see LAI range in Table 1) it is likely that rooting depth varies with different growth phases, and thus the connection between *ET* and deeper layer soil moisture in the model may be overstated for periods of sparse vegetation cover. This may also explain the excessive reduction in root-zone soil moisture from LEH_Assim and Tsk_Assim in the first half of the year, coinciding with reductions in *ET* (Figs. 2a–3a and 2c–3c). These errors are likely to be quite intricate and require more detailed data than is available here to properly address. It is also worth noting that in this respect uncertainties in the subsurface (soil properties, root water extraction profiles, etc.) are severe. Progress in this area may result in more accurate estimates of error covariances and hence better assimilation outcomes overall.

7. Conclusions

This paper has presented one-dimensional Open-Loop and various data assimilation runs of the CBM for a temperate grassland site in southern New South Wales, Australia. Comparisons between Open-Loop and validation data suggest that accurate modelling of heat fluxes is most difficult for water limited scenarios where *ET* rates are below potential. This is evident from the poorer Open-Loop predictions of *ET* in the first ~60 days of the year spanning late summer and through all of autumn where the soil profile is mostly at its driest, and for a period towards the end of the year around the spring/summer transition where moisture storage is below maximum. Exact causes of the poorer predictions are likely to be varied, including parameter uncertainty, model structural limitations, and possibly isolated instances of groundwater contribution where rainfall forcing data may not have accounted for the total water supply for the LSM water balance.

Five different assimilation runs were conducted using real field data for a selection of times corresponding to approximate satellite overpasses relevant to each data type: latent and sensible heat (LEH_Assim); 0–8 cm soil moisture (SM_Assim); skin temperature (Tsk_Assim); all four of these (ALL_Assim); and 0–8 cm soil moisture combined with skin temperature (SMTsk_Assim). It was demonstrated that the multi-observation approach of SMTsk_Assim produced the greatest improvements to *ET* relative to validation data constructed from independent field observations. This is to be contrasted with the traditional SM_Assim approach which led to the strongest root-zone soil moisture improvements but with relatively modest *ET* improvements. Thus accurate root-zone soil moisture prediction does not necessarily translate to optimal heat fluxes.

The LEH_Assim approach made strong improvements to *ET* as expected, second only to those from SMTsk_Assim. From a remote sensing perspective this implies that incorporating skin temperature from thermal imagery together with soil moisture observations in the data assimilation may be more beneficial to LSM heat flux accuracy than assimilating *LE* and *H* alone, which first needs to be derived using the same thermal imagery via a separate energy balance model. A major strength of SMTsk_Assim in this study was in balancing impacts on the model energy and water balances to improve both soil moisture and temperature states in addition to *ET*.

Consequently, this study demonstrates the value of multi-observation assimilation into a LSM using real observations. This provides a sound basis for further multi-observation assimilation studies using remotely sensed data products, including remotely sensed *LE* and *H* assimilation, to better understand and draw stronger conclusions about its potential benefits.

Acknowledgements

An Australian Postgraduate Award (APA) Scholarship from the Australian Federal Government provided the funds for the lead author Robert Pipunic to undertake this work as part of his PhD research. While at The University of Melbourne, Cressida Savige provided invaluable help in the initial set-up of the eddy covariance system and supporting instrumentation. A University of Melbourne–CSIRO collaborative research grant provided funds for maintenance of the Kyeamba Creek flux station site including operational support for Robert Pipunic's PhD work. The authors sincerely thank Fred Hulm, who allowed the Kyeamba Creek flux station to be installed on his property.

We are extremely grateful to Dongryeol Ryu from the Department of Infrastructure Engineering at The University of Melbourne, Australia, who made time for valuable feedback and provided important advice on key technical aspects of the research methodology. Thanks are also due to Vanessa Haverd at the CSIRO Land and Water division in Canberra, Australia, for helpful comments on the manuscript. From the same division, Tim McVicar provided the fPAR data product for deriving LAI values used in simulations. Ying-Ping Wang at the

CSIRO Marine and Atmospheric Research division in Aspendale, Australia, provided the CBM code along with helpful advice.

References

- Abramowitz, G. (2006). *User guide for the Community Atmosphere Biosphere Land Exchange (CABLE) land surface model*. Aspendale, Australia: CSIRO Marine and Atmospheric Research.
- Allen, R. G., Tasumi, M., & Trezza, R. (2007). Satellite-based energy balance for mapping evapotranspiration with internalized calibration (METRIC): Model. *Journal of Irrigation and Drainage Engineering*, 133, 380–394.
- Anderson, J. L., & Anderson, S. L. (1999). A Monte Carlo implementation of the nonlinear filtering problem to produce ensemble assimilations and forecasts. *Monthly Weather Review*, 127, 2741–2758.
- Balsamo, G., Mahfouf, J.-F., Belair, S., & Deblonde, G. (2007). A land data assimilation system for soil moisture and temperature: An information content study. *Journal of Hydrometeorology*, 8, 1225–1242.
- Bastiaanssen, W. G. M., Menenti, M., Feddes, R. A., & Holtslag, A. A. M. (1998). A remote sensing surface energy balance algorithm for land (SEBAL) 1. Formulation. *Journal of Hydrology*, 212–213, 198–212.
- Beljaars, A. C. M., Viterbo, P., Miller, M. J., & Betts, A. K. (1996). The anomalous rainfall over the United States during July 1993: Sensitivity to land surface parameterization and soil moisture anomalies. *Monthly Weather Review*, 124, 362–383.
- Campbell Scientific Inc. (1996). *CS615 Water content reflectometer*. Instruction manual. Logan, Utah, USA: Campbell Scientific Inc.
- Campbell Scientific Inc. (1998). *CSAT Three dimensional sonic anemometer*. Instruction manual. Logan, Utah, USA: Campbell Scientific Inc.
- Campbell Scientific Inc. (1999). *HFT3 Soil heat flux plate*. Instruction manual. Logan, Utah, USA: Campbell Scientific Inc.
- Carlson, T. N., & Ripley, D. A. (1997). On the relation between NDVI, fractional vegetation cover, and Leaf Area Index. *Remote Sensing of Environment*, 62, 241–252.
- Case, J. L., Crosson, W. L., Kumar, S. V., Lapenta, W. M., & Peters-Lidard, C. D. (2008). Impacts of high-resolution land surface initialization on regional sensible weather forecasts from the WRF model. *Journal of Hydrometeorology*, 9, 1249–1266.
- Chen, F., Manning, K. W., LeMone, M. A., Trier, S. B., Alfieri, J. G., Roberts, R., et al. (2007). Description and evaluation of the characteristics of the NCAR high-resolution land data assimilation system. *Journal of Applied Meteorology and Climatology*, 46, 694–713.
- Chen, X. Y., & McKane, D. J. (1997). *Soil landscapes of the Wagga Wagga 1:100 000 sheet*. Soil landscape series report. Sydney, Australia: Department of Land and Water Conservation.
- Chen, F., Pielke, R. A., Sr., & Mitchell, K. (2001). Development and application of land surface models for mesoscale atmospheric models: Problems and promises. In V. Lakshmi, J. D. Albertson, & J. Schaake (Eds.), *Land surface hydrology, meteorology, and climate: Observations and modeling* (pp. 107–135). Washington, DC: American Geophysical Union.
- Choudhury, B. J. (1989). Estimating evaporation and carbon assimilation using infrared temperature data: Vistas in modeling. In G. Asrar (Ed.), *Theory and applications of optical remote sensing* (pp. 628–690). New York: John Wiley and Sons.
- CSIRO (2007). *Soil particle analysis*. Report R0710062. Perth, Australia: CSIRO Division of Minerals Particle Analysis Service.
- de Rosnay, P., Drusch, M., Vasiljevic, D., Balsamo, G., Albergel, C., & Isaksen, L. (2012). A simplified Extended Kalman Filter for the global operational soil moisture analysis at ECMWF. *Quarterly Journal of the Royal Meteorological Society*, 138.
- Denman, K. L., Brasseur, G., Chidthaisong, A., Ciais, P., Cox, P. M., Dickinson, R. E., et al. (2007). Couplings between changes in the climate system and biogeochemistry. In S. Solomon, D. Qin, M. Manning, Z. Chen, M. Marquis, K. B. Averyt, M. M. B. Tignor, & H. L. Miller (Eds.), *Climate change 2007: The physical science basis. Contribution of Working Group I to the Fourth Assessment Report of the Intergovernmental Panel on Climate Change* (pp. 499–568). Cambridge, United Kingdom and New York, NY, USA: Cambridge University Press.
- Dharssi, I., Bovis, K. J., Macpherson, B., & Jones, C. P. (2011). Operational assimilation of ASCAT surface soil wetness at the Met Office. *Hydrology and Earth System Sciences*, 15, 2729–2746.
- Donohue, R. J., Roderick, M. L., & McVicar, T. R. (2008). Deriving consistent long-term vegetation information from AVHRR reflectance data using a cover-triangle-based framework. *Remote Sensing of Environment*, 112, 2938–2949.
- Douville, H., Viterbo, P., Mahfouf, J.-F., & Beljaars, A. C. M. (2000). Evaluation of the optimum interpolation and nudging techniques for soil moisture analysis using FIFE data. *Monthly Weather Review*, 128, 1733–1756.
- Draper, C. S., Mahfouf, J.-F., & Walker, J. P. (2009). An EKF assimilation of AMSR-E soil moisture into the ISBA land surface scheme. *Journal of Geophysical Research-Atmospheres*, 114, D20104.
- Draper, C. S., Walker, J. P., Steinle, P., Jeu, R. d., & Holmes, T. (2009). An evaluation of AMSR-E derived soil moisture over Australia. *Remote Sensing of Environment*, 113, 703–710.
- Drusch, M., Wood, E. F., & Gao, H. (2005). Observation operators for the direct assimilation of TRMM microwave imager retrieved soil moisture. *Geophysical Research Letters*, 32, L15403.
- Entekhabi, D., Nakamura, H., & Njoku, E. G. (1994). Solving the inverse problem for soil moisture and temperature profiles by sequential assimilation of multifrequency remotely sensed observations. *IEEE Transactions on Geoscience and Remote Sensing*, 32, 438–448.
- Evensen, G. (1994). Sequential data assimilation with a nonlinear quasi-geostrophic model using Monte Carlo methods to forecast error statistics. *Journal of Geophysical Research—Oceans*, 99, 10143–10162.
- Gao, H., Wood, E. F., Jackson, T. J., Drusch, M., & Bindlish, R. (2006). Using TRMM/TMI to retrieve surface soil moisture over the southern United States from 1998 to 2002. *Journal of Hydrometeorology*, 7, 23–38.
- Hain, C. R., Crow, W. T., Anderson, M. C., & Mecikalski, J. R. (2012). An ensemble Kalman filter dual assimilation of thermal infrared and microwave satellite observations of soil moisture into the Noah land surface model. *Water Resources Research*, 48, W11517.
- Huang, C., Li, X., & Lu, L. (2008). Retrieving soil temperature profile by assimilating MODIS LST products with ensemble Kalman filter. *Remote Sensing of Environment*, 112, 1320–1336.
- Imaoka, K., Kachi, M., Kasahara, M., Ito, N., Nakagawa, K., & Oki, T. (2010). Instrument performance and calibration of AMSR-E and AMSR2. *International Archives of the Photogrammetry, Remote Sensing and Spatial Information Sciences*, XXXVIII, 13–16.
- Kaleita, A. L., & Kumar, P. (2000). AVHRR estimates of surface temperature during the Southern Great Plains 1997 experiment. *Journal of Geophysical Research*, 105, 20791–20801.
- Kalma, J. D., McVicar, T. R., & McCabe, M. F. (2008). Estimating Land Surface Evaporation: A Review of Methods Using Remotely Sensed Surface Temperature Data. *Surveys in Geophysics*, 29, 421–469.
- Kerr, Y. H. (2001). Soil moisture retrieval from space: The Soil Moisture and Ocean Salinity (SMOS) mission. *IEEE Transactions on Geoscience and Remote Sensing*, 39, 1729–1735.
- Koster, R. D., & Milly, P. C. D. (1997). The interplay between transpiration and runoff formulations in land surface schemes used with atmospheric models. *Journal of Climate*, 10, 1578–1591.
- Koster, R. D., Suarez, M. J., Liu, P., Jambor, U., Berg, A., Kistler, M., et al. (2004). Realistic initialization of land surface states: Impacts on subseasonal forecast skill. *Journal of Hydrometeorology*, 5, 1049–1063.
- Kowalczyk, E. A., Wang, Y. P., Law, R. M., Davies, H. L., McGregor, J. L., & Abramowitz, G. (2006). *The CSIRO Atmosphere Biosphere Land Exchange (CABLE) model for use in climate models and as an offline model*. Paper 013. Aspendale, Australia: CSIRO Marine and Atmospheric Research.
- Kumar, S. V., Reichle, R. H., Koster, R. D., Crow, W. T., & Peters-Lidard, C. D. (2009). Role of subsurface physics in the assimilation of surface soil moisture observations. *Journal of Hydrometeorology*, 10, 1534–1547.
- Lakshmi, V. (2000). A simple surface temperature assimilation scheme for use in land surface models. *Water Resources Research*, 36, 3687–3700.
- Law, R. M., Raupach, M. R., Abramowitz, G., Dharssi, I., Haverd, V., Pitman, A. J., et al. (2012). The Community Atmosphere Biosphere Land Exchange (CABLE) model Roadmap for 2012–2017. The Centre for Australian Weather and Climate Research (CAWCR), Technical Report 057.
- Li, J., & Islam, S. (1999). On the estimation of soil moisture profile and surface fluxes partitioning from sequential assimilation of surface layer soil moisture. *Journal of Hydrology*, 220, 86–103.
- LI-COR Inc. (2003). *LI-7500 CO2/H2O analyzer*. Instruction manual. Lincoln, Nebraska, USA: LI-COR Inc.
- Lu, H., Raupach, M. R., McVicar, T. R., & Barrett, D. J. (2003). Decomposition of vegetation cover into woody and herbaceous components using AVHRR NDVI time series. *Remote Sensing of Environment*, 86, 1–18.
- Mahfouf, J.-F. (1991). Analysis of soil moisture from near-surface parameters: A feasibility study. *Journal of Applied Meteorology*, 30, 1534–1547.
- Mahfouf, J.-F. (2010). Assimilation of satellite-derived soil moisture from ASCAT in a limited-area NWP model. *Quarterly Journal of the Royal Meteorological Society*, 136, 784–798.
- McKenzie, N., Gallant, J., & Gregory, L. (2003). *Estimating water storage capacities in soil at catchment scales*. Technical Report 03/3. Australia: Cooperative Research Centre for Catchment Hydrology.
- McKenzie, N. J., Jacquier, D. W., Ashton, L. J., & Cresswell, H. P. (2000). *Estimation of soil properties using the Atlas of Australian Soils*. Technical Report 11/00. Canberra, Australia: CSIRO Land and Water.
- McNider, R. T., Song, A. J., Casey, D. M., Wetzal, P. J., Crosson, W. L., & Rabin, R. M. (1994). Toward a dynamic-thermodynamic assimilation of satellite surface temperature in numerical atmosphere models. *Monthly Weather Review*, 122, 2784–2803.
- McVicar, T. R., Jupp, D. L. B., Reece, P. H., & Williams, N. A. (1996). *Relating Landsat TM vegetation indices to in-situ Leaf Area Index measurements*. Technical memorandum 96.14. Australia: CSIRO Division of Water Resources.
- Meng, C. L., Li, Z.-L., Zhan, X., Shi, J. C., & Liu, C. Y. (2009). Land surface temperature data assimilation and its impact on evapotranspiration estimates from the Common Land Model. *Water Resources Research*, 45, W02421.
- Njoku, E. G., & Entekhabi, D. (1995). Passive microwave remote sensing of soil moisture. *Journal of Hydrology*, 184, 101–130.
- Owe, M., Dejeu, R. A. M., & Holmes, T. R. H. (2008). Multi-sensor historical climatology of satellite-derived global land surface moisture. *Journal of Geophysical Research*, 113, F01002.
- Pan, M., Wood, E. F., Wojcik, R., & McCabe, M. F. (2008). Estimation of regional terrestrial water cycle using multi-sensor remote sensing observations and data assimilation. *Remote Sensing of Environment*, 112, 1282–1294.
- Pipunic, R. C., Walker, J. P., & Western, A. W. (2008). Assimilation of remotely sensed data for improved latent and sensible heat flux prediction: A comparative synthetic study. *Remote Sensing of Environment*, 112, 1295–1305.
- Potter, C. S., Randerson, J. T., Field, C. B., Matson, P. A., Vitousek, P. M., Mooney, H. A., et al. (1993). Terrestrial ecosystems production: A process model based on global satellite and surface data. *Global Biogeochemical Cycles*, 7, 811–841.
- Raupach, M. R., Finkele, K., & Zhang, L. (1997). SCAM (Soil-Canopy-Atmosphere Model): Description and comparison with field data. *Technical report*, 132, CSIRO Centre for Environmental Mechanics.
- Reichle, R. H., Crow, W. T., Koster, R. D., Sharif, H. O., & Mahanama, S. P. P. (2008). Contribution of soil moisture retrievals to land data assimilation products. *Geophysical Research Letters*, 35, L01404.

- Reichle, R. H., & Koster, R. D. (2004). Bias reduction in short records of satellite soil moisture. *Geophysical Research Letters*, 31, L19501.
- Reichle, R. H., & Koster, R. D. (2005). Global assimilation of satellite surface soil moisture retrievals into the NASA Catchment land surface model. *Geophysical Research Letters*, 32, L02404.
- Reichle, R. H., Koster, R. D., Liu, P., Mahanama, S. P. P., Njoku, E. G., & Owe, M. (2007). Comparison and assimilation of global soil moisture retrievals from the Advanced Microwave Scanning Radiometer for the Earth Observing System (AMSR-E) and the Scanning Multichannel Microwave Radiometer (SMMR). *Journal of Geophysical Research*, 112, D09108.
- Reichle, R. H., Kumar, S. V., Mahanama, S. P. P., Koster, R. D., & Liu, Q. (2010). Assimilation of satellite-derived skin temperature observations into land surface models. *Journal of Hydrometeorology*, 11, 1103–1122.
- Rhodin, A., Kucharski, F., Callies, U., Eppel, D. P., & Wergen, W. (1999). Variational analysis of effective soil moisture from screen-level atmospheric parameters: Application to a short-range weather forecast model. *Quarterly Journal of the Royal Meteorological Society*, 125, 2427–2448.
- Sabater, J. M., Rudiger, C., Calvet, J. -C., Fritz, N., Jarlan, L., & Kerr, Y. -H. (2008). Joint assimilation of surface soil moisture and LAI observations into a land surface model. *Agricultural and Forest Meteorology*, 148, 1362–1373.
- Schuurmans, J. M., Troch, P. A., Veldhuizen, A. A., Bastiaanssen, W. G. M., & Bierkens, M. F. P. (2003). Assimilation of remotely sensed latent heat flux in a distributed hydrological model. *Advances in Water Resources*, 26, 151–159.
- Seuffert, G., Wilker, H., Viterbo, P., Drusch, M., & Mahfouf, J. -F. (2004). The usage of screen-level parameters and microwave brightness temperature for soil moisture analysis. *Journal of Hydrometeorology*, 5, 516–531.
- Siriwardena, L., Chiew, F., Richter, H., & Western, A. W. (2003). *Preparation of a climate data set for the Murrumbidgee River catchment for land surface modelling experiments*. Working Document 03/1. Melbourne, Australia: Cooperative Research Centre for Catchment Hydrology.
- Smith, A. B., Walker, J. P., Western, A. W., Young, R. I., Ellet, K. M., Pipunic, R. C., et al. (2012). The Murrumbidgee soil moisture monitoring network data set. *Water Resources Research*, 48, W07701.
- Sobrino, J. A., Jimenez-Munoz, J. C., & Paolini, L. (2004). Land surface temperature retrieval from LANDSAT TM 5. *Remote Sensing of Environment*, 90, 434–440.
- Soil Moisture Equipment Corp. (1989). *TRASE system 1 operating instructions*. Santa Barbara, California, USA: Soil Moisture Equipment Corp.
- Su, Z. (2002). The Surface Energy Balance System (SEBS) for estimation of turbulent heat fluxes. *Hydrology and Earth System Sciences*, 6, 85–99.
- Su, C. -H., Ryu, D., Young, R. I., Western, A. W., & Wagner, W. (2013). Inter-comparison of microwave satellite soil moisture retrievals over the Murrumbidgee Basin, southeast Australia. *Remote Sensing of Environment*, 134, 1–11.
- Sun, D., Pinker, R. T., & Basara, J. B. (2004). Land surface temperature estimation from the next generation of Geostationary Operational Environmental Satellites: GOES M-Q. *Journal of Applied Meteorology*, 43, 363–372.
- Turner, M. R. J., Walker, J. P., & Oke, P. R. (2008). Ensemble member generation for sequential data assimilation. *Remote Sensing of Environment*, 112, 1421–1433.
- Twine, T. E., Kustas, W. P., Norman, J. M., Cook, D. R., Houser, P. R., Meyers, T. P., et al. (2000). Correcting eddy covariance flux underestimates over a grassland. *Agricultural and Forest Meteorology*, 103, 279–300.
- Unidata Australia (1997). *STARLOG Temperature probes*. User manual supplement. Australia: MacLaren Enterprises.
- Viterbo, P., & Beljaars, A. C. M. (1995). An improved land surface parameterization scheme in the ECMWF model and its validation. *Journal of Climate*, 8, 2716–2748.
- Wagner, W., Lemoine, G., & Rott, H. (1999). A method for estimating soil moisture from ERS scatterometer and soil data. *Remote Sensing of Environment*, 70, 191–207.
- Walker, J. P., & Houser, P. R. (2004). Requirements of a global near-surface soil moisture satellite mission: Accuracy, repeat time, and spatial resolution. *Advances in Water Resources*, 27, 785–801.
- Walker, J. P., Willgoose, G. R., & Kalma, J. D. (2001a). One-dimensional soil moisture profile retrieval by assimilation of near-surface measurements: A simplified soil moisture model and field application. *Journal of Hydrometeorology*, 2, 356–373.
- Walker, J. P., Willgoose, G. R., & Kalma, J. D. (2001b). One-dimensional soil moisture profile retrieval by assimilation of near-surface observations: A comparison of retrieval algorithms. *Advances in Water Resources*, 24, 631–650.
- Wan, Z., & Dozier, J. (1996). A generalized split-window algorithm for retrieving land-surface temperature from space. *IEEE Transactions on Geoscience and Remote Sensing*, 34, 892–905.
- Wan, Z., & Li, Z. -L. (1997). A physics-based algorithm for retrieving land-surface emissivity and temperature from EOS/MODIS data. *IEEE Transactions on Geoscience and Remote Sensing*, 35, 980–996.
- Wang, Y. P., Baldocchi, D., Leuning, R., Falge, E., & Vesala, T. (2007). Estimating parameters in a land surface model by applying non-linear inversion to eddy covariance flux measurements from eight FLUXNET sites. *Global Change Biology*, 13, 652–670.
- Wang, Y. P., Kowalczyk, E., Leuning, R., Abramowitz, G., Raupach, M. R., Pak, B., et al. (2011). Diagnosing errors in a land surface model (CABLE) in the time and frequency domains. *Journal of Geophysical Research*, 116, <http://dx.doi.org/10.1029/2010JG001385>.
- Wang, Y. P., & Leuning, R. (1998). A two-leaf model for canopy conductance, photosynthesis and partitioning of available energy I. Model description and comparison with a multi-layered model. *Agricultural and Forest Meteorology*, 91, 89–111.
- Wang, Y. P., Leuning, R., Cleugh, H. A., & Coppin, P. A. (2001). Parameter estimation in surface exchange models using non-linear inversion: How many parameters can we estimate and which measurements are most useful? *Global Change Biology*, 7, 495–510.
- Wang, K., & Liang, S. (2009). Evaluation of Aster and MODIS land surface temperature and emissivity products using long-term surface longwave radiation observations at SURFRAD sites. *Remote Sensing of Environment*, 113, 1556–1565.
- Western, A. W., & Seyfried, M. S. (2005). A calibration and temperature correction procedure for the water-content reflectometer. *Hydrological Processes*, 19, 3785–3793.
- Kipp, & Zonen, B. V. (2002). *CNR1 net radiometer*. Instruction manual. Delft, The Netherlands: Kipp and Zonen B.V.